Journal of Alloys and Compounds 861 (2021) 157938

Contents lists available at ScienceDirect

Journal of Alloys and Compounds

journal homepage: http://www.elsevier.com/locate/jalcom

# Solid-state synthesis, rotatable magnetic anisotropy and characterization of $Co_{1-x}Pt_x$ phases in 50Pt/50fccCo(001) and 32Pt/68fccCo(001) thin films

V.G. Myagkov [a, *], L.E. Bykova [a], V.S. Zhigalov [a], A.A. Matsynin [a], D.A. Velikanov [a], G.N. Bondarenko [b]

[a] Kirensky Institute of Physics, Federal Research Center KSC SB RAS, Krasnoyarsk, Russian Federation
[b] Institute of Chemistry and Chemical Technology, Federal Research Center KSC SB RAS, Krasnoyarsk, Russian Federation

ARTICLE INFO

*Article history:*
Received 13 July 2020
Received in revised form
2 November 2020
Accepted 10 November 2020
Available online 17 November 2020

*Keywords:*
$L1_0$-CoPt
Hard magnetic
Thin-film solid-state reactions
Rotatable magnetic anisotropy
Magnetic-field-induced twining
Co-Pt phase Diagram

ABSTRACT

We reported the phase formation sequences in 50Pt/50fcc-Co(001) and 32Pt/68fcc-Co(001) thin films after annealing up to 850 °C. In both cases, the ordered $L1_0$ phase formed first on the Pt/Co interface at ~400 °C and as the annealing temperature increased the $L1_0$ phase transformed into the chemically disordered fcc A1 phase in 50Pt/50fcc-Co(001) at 750 °C and in 32Pt/68fcc-Co(001) films at 550 °C. Based on the analysis of solid-state reactions in thin films, a phase transition at ~ 400 °C is predicted in Co-Pt systems with a 32–72% Pt composition. Torque measurements of the 50Pt/50fcc-Co(001) samples showed that the rotatable magnetic anisotropy coexisted with the three variants of $L1_0$ in a temperature range of 400–750 °C. An analysis of the torque curves revealed that the $L1_0$ films consist of a soft magnetic layer epitaxially intergrown to the substrate MgO(001) and a top layer having rotatable magnetic anisotropy. It showed that the magnetically hard properties of $L1_0$ films are associated with a rotatable magnetic anisotropy layer. A model of rotatable magnetic anisotropy is reasoned, which is founded on some identical mechanisms of rotatable magnetic anisotropy and magnetic-field-induced strains, explaining the ferromagnetic shape-memory effect in Heusler alloys. Our results suggested that the rotatable magnetic anisotropy phenomena may have an important role in the origin of perpendicular anisotropy in hard magnetic $L1_0$ structures.



## 1. Introduction

$Co_{1-x}Pt_x$ alloy thin films attracts a lot of attention because they have a wide concentration range with high perpendicular magnetic anisotropy (PMA) which is important for many spintronic applications [1]. In particular, the stable ordered $L1_0$-CoPt [2] and metastable ordered $L1_1$-CoPt, Bh-CoPt, $D0_{19}$-$Co_3Pt$ [2,3] phases possessing uniaxial magnetocrystalline anisotropy energies $K_u > 10^7$ erg/cm$^3$, which are the main source of PMA. However, PMA is also observed in the cubic $L1_2$-$CoPt_3$ [4] thin films in which PMA is not expected. In addition, the mechanisms of the appearance of PMA in $Co_xPt_{1-x}$ films deposited on amorphous substrates [5] in nanopatterned [6] and in disordered A1-CoPt films [7] are not clear. The Co/Pt multilayers also possessed PMA [8–10] and the alloying between the Co and Pt is assumed to lie on the PMA basis [8,9]. This suggested that mechanisms other than magnetocrystalline nature explains the origin of the giant PMA e.g., the formation of the column structure, the preferable location of the Co–Pt bonds perpendicular to the substrate, the existence of planar stress, interfacial magnetic anisotropy, etc. In addition, an understanding of the real nature of PMA is complicated by the presence of high rotatable magnetic anisotropy (RMA) in hard magnetic $L1_0$-CoPt [11,12], $L1_0$-FePt [13], $Tb_{25}Fe_{75}$ [14], δ-$Mn_{0.6}Ga_{0.4}$ [15] and in MnBi [16] thin films. Historically, Park et al. first reported the RMA phenomenon in $Co_{0.47}Pt_{0.53}$ alloy films in which the location of the easy axis is not clear for samples annealed above 500 °C [11]. The RMA phenomenon consists of the magnetization easy axis rotating behind a rotating magnetic field in the fields exceeding the coercive force $H > H_c$, which can exceed 10 kOe for magnetically hard films. The main techniques for studying RMA in thin films are; using a torque magnetometer [11–16], ferromagnetic resonance [18], a vector network analyzer [19], Brillouin light scattering [17] and

* Corresponding author.
*E-mail address:* miagkov@iph.krasn.ru (V.G. Myagkov).

https://doi.org/10.1016/j.jallcom.2020.157938
0925-8388/

magnetic force microscopy [20]. Unlike other kinds of anisotropies, the rotatable magnetic anisotropy is not described by a sinusoidal law and, therefore, has no unambiguous characteristic. The difference $H_{rot} = H_k^{dyn} - H_k^{stat}{}_{rot}$ between the dynamic field and the static field of the magnetic anisotropy, measured by ferromagnetic resonance, is used to characterize the RMA [for example 17–19]. In torque measurements, the RMA can be characterized by the average torque constant $L^{rot}$ at large rotational angles of the magnetic field [12,13]. At the out-of-plane rotation of the magnetic field, the torque curves $L\perp(\phi)$ contains the $L\perp^{rot}$ contributions from RMA and the form anisotropy. Therefore, for samples having an $L\perp^{rot}$ constant exceeding the form anisotropy, the easy axis can be aligned in any spatial direction, such as in a plane and perpendicular to the plane of the sample [12,13]. The RMA samples showed the equality of the out-of-plane $L\perp^{rot}$ and in-plane $L_{||}^{rot}$ torque constants $L\perp^{rot} = L_{||}^{rot}$ and close or identical out-of-plane $H_c\perp$ and in-plane $H_c^{||}$ hysteresis loops, having coercivity $H_c\perp = H_c^{||}$, which is the spatial characteristic of RMA [12–16]. A literature review showed that some Co-Pt alloy thin films possessed these characteristics [21–26], and this suggested that they also have a large RMA. Various techniques were used to create the $Co_{1-x}Pt_x$ thin films, such as rf-magnetron sputtering [27], dc-magnetron sputtering [28], molecular beam epitaxy [29] and pulsed laser deposition [30]. However, the magnetic and structural properties of the $Co_{1-x}Pt_x$ films, depends on the composition, long-range-order parameter degree, preparation method and heat treatment conditions. The chemical interactions of Pt with hexagonal hcp-Co, the cubic fcc-Co modifications, the phase sequences, the structural and magnetic characteristics of the reaction products arising from solid-state reaction as well as the conditions and nature of PMA formation remain unknown.

It is well known that early studies of solid-state reactions in thin films showed that at a certain temperature $T_{in}$ (initiation temperature) only one phase is formed, which is called the first phase. As the annealing temperature increases, other phases can also arise with the formation of a phase sequence [31–34]. Our previous studies and analysis of solid-state reactions for many bilayer films showed that the initiation temperatures $T_{in}$ coincided with the temperatures $T_K$ of the structural phase transformations ($T_{in} = T_K$) in these binary systems. In particular, the initial temperatures $T_{in}$ (Cu/Au) and $T_{in}$ (Ni/Fe) of reactions in Cu/Au and Ni/Fe films coincided with the minimum temperature of 240 °C of the order – disorder phase transition in Cu – Au [35,36] and with the temperature of 350 °C of eutectoid decomposition in the Fe–Ni systems [37,38], respectively. The reactions in Ni/Al, Ti/Ni and Cd/Au bilayers started at 180 °C, ~ 100 °C and 67 °C, which match with temperatures of the reverse martensitic transformations, respectively, in Ni-Al [39], Ti-Ni [40] and Cd-Au [41] binary systems. The equality $T_{in} = T_K$ was also found for the eutectic reactions (420 °C) in Al/Ge [42], the superionic transition (150 °C) in Se/Cu [43], the spinodal decomposition in Mn/Ge (120 °C) [44,45] bilayers and other phase transformations [15,46–49]. In summary, the equality $T_{in} = T_k$ indicated that low-temperature solid-state thin-film reactions in A/B bilayers occurred only in A-B binary systems, which have corresponding low-temperature solid-state transformations.

This work has two main objectives: the first step is to study of interfacial reactions in 50Pt/50fccCo(001) and 32Pt/68fccCo(001) bilayers to clarify of the Co-rich part the Co-Pt phase diagram, the next step is to suggest the RMA model based on characteristic features of the rotatable anisotropy in the $L1_0$-$Pt_{50}Co_{50}$(001) films. Using X-ray diffraction and magnetic torque curve studies, we found that RMA is associated with the surface layer of the synthesized epitaxial $L1_0$-$Pt_{50}Co_{50}$(001) film. An important consequence of this work is to substantiate general magnetic-field-induced twining mechanism controlling both the RMA phenomena and large strains in Heusler alloys. From the above it follows that RMA can play a significant role in the nature of PMA and therefore, studies of the RMA formation conditions under various technological conditions is necessary.

## 2. Experiment

The preparation of the initial Pt/fcc-Co(001) bilayers was described in detail in this work [26]. In the first step, the epitaxial fcc-Co(001) layer was deposited on the MgO(001) substrate at a pressure of $10^{-5}$ Torr and a temperature of 250 °C. Under such deposition conditions the fcc-Co(001) layer forms the cube-on-cube orientation relationship fccCo(001)[100]||MgO(001)[100]. The fcc-Co(001)/MgO(001) films had a saturation magnetization of ~ 1410 emu/cm$^3$ and a four-fold magnetic anisotropy with the $K_4$ constant coinciding with the first magnetocrystalline anisotropy constant of the epitaxial fcc-Co(001) layer ($K_1^{fcc-Co}$ = - 5.5 × $10^5$ erg/cm$^3$) [50]. The $K_1^{fcc-Co}$ is negative because the easy magnetization axes coincided with the [110] and [1-10] directions of the fcc-Co(001) film and the MgO(001) substrate. In the second step, the top Pt layer was deposited at room temperature to prevent a reaction between the Pt and Co during the deposition. Samples of 50Pt/50fcc-Co(001)/MgO(001) and 32Pt/68fcc-Co(001)/MgO(001) with stoichiometries of $Co_{50}Pt_{50}$ and $Co_{68}Pt_{32}$ respectively, determined by EDS microanalysis, and up to 300 nm total thickness were used for the experiments. The initial samples of 50Pt/50fcc-Co(001)/MgO(001) and 32Pt/68fcc-Co(001)/MgO(001) were annealed for 1 h from 50 °C to 850 °C with a step of 50 °C. The magnetic four-fold anisotropy constants $K_4^0$ was determined for the total volume of the 50Pt/50fcc-Co(001) and 32Pt/68fcc-Co(001) bilayers, which turned out to be $K_4^0 = 3.0 \cdot 10^5$ erg/cm$^3$ and $K_4^0 = 3.4 \cdot 10^5$ erg/cm$^3$, respectively. The formed phases were identified with a DRON-4-07 diffractometer (Cu$K_\alpha$ radiation). The saturation magnetization $M_S$ and the coercivity $H_c$ were measured using a vibration magnetometer in magnetic fields up to 22 kOe. Torque magnetometer measurements were used, because it is a powerful method for determining RMA and the classical magnetic anisotropies $K_0 \cdot \mathrm{Sin}(\phi+\gamma_1)$, $K_u \cdot \mathrm{Sin}(2\phi+\gamma_2)$, $K_4 \cdot \mathrm{Sin}(4\phi+\gamma_4)$, . $K_n \cdot \mathrm{Sin}(n\phi+\gamma_n)$ analyzing the location of the easy axes ($\gamma_1, \gamma_2, \gamma_4 \ldots \gamma_n$) angles in magnetic materials. Torque curves were measured using a torque magnetometer with a sensitivity of $3.76 \cdot 10^{-9}$ Nm and a maximum magnetic field of 12 kOe. All measurements were performed at room temperature.

## 3. Results

### 3.1. Phase transformations and RMA in 50Pt/50fcc-Co(001) thin films

Fig. 1 represents the X-ray-diffraction results (Fig. 1a) and relevant torque curves (Fig. 1b) of 50Pt/50fcc-Co(001) films during thermal annealing at temperatures ranging from room temperature to 850 °C. As shown in Fig. 1a the XRD profiles of the as-deposited film contain only the (200) fcc-Co reflection, which denotes the epitaxial growth of the fcc-Co(001) layer on the MgO(001) surface at 250 °C. The absence of Pt peaks means that the Pt is finely dispersed after deposition on a fcc-Co (001) layer at room temperature. The X-ray patterns did not change when annealed to 400 °C, which is indicative of the absence of mixing and formation of new phases at the Pt/Co interface. After annealing at 400 °C, the strong (200) fcc-Co peak began decreasing and disappeared after 550 °C. Instead, the wide and very weak superstructural (001)$L1_0$, fundamental (002)$L1_0$ and (200)$L1_0$ reflections appeared after annealing above 400 °C, which are a sign of the start of the reaction between Pt and Co and the synthesis of a thin low crystalline

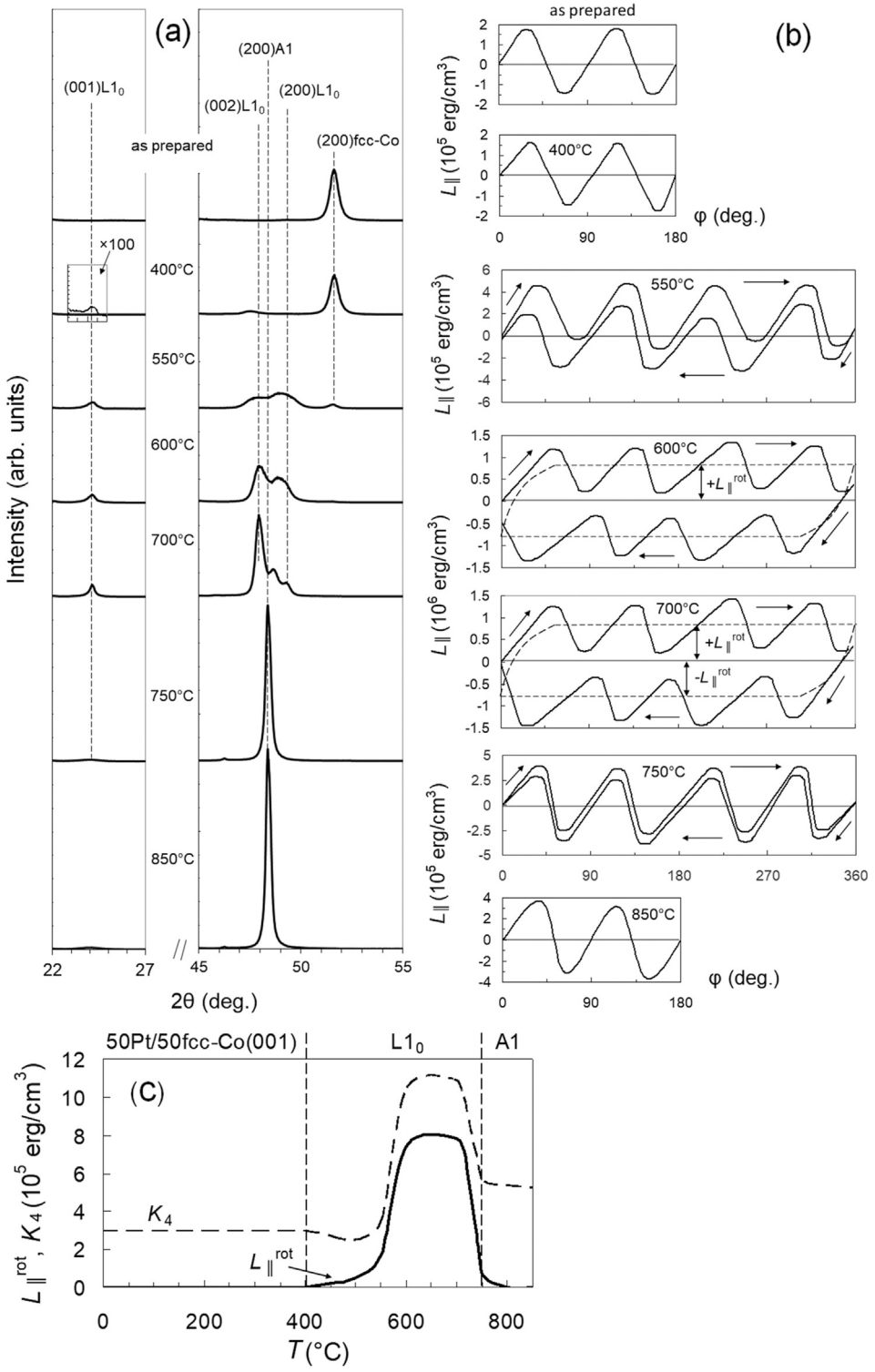


**Fig. 1.** X-ray diffraction patterns (a) and relevant in-plane torque curves (b) showing the sequential synthesis of $L1_0$ and A1-$Co_{50}Pt_{50}$ in epitaxial 50Pt/50Co(001) thin films under annealing temperatures from room temperature up to 850 °C. (c) The temperature dependence of $L_{\parallel}^{rot}$ and the four-fold $K_4$ constants confirming the simultaneous formation of $L1_0$ and RMA between 400 °C and 750 °C.

quality epitaxial ordered $L1_0$ layer at the Pt/Co interface. The (001) $L1_0$ and (002)$L1_0$ reflections were broadened, which indicated significant lattice distortions in the forming of $L1_0$ layer (defective layer). After annealing above 550 °C the (001)$L1_0$ and (002)$L1_0$, reflections grew, which resulted to an increase in the thickness and crystalline quality of the $L1_0$layer. As previously known, the highly coercive $L1_0$-ordered FePt, CoPt, FePd thin films prepared on MgO(001) by various methods formed the three equivalent X-,Y-, Z-variants of $L1_0$, which have epitaxial orientation relationships (1) with the substrates [51,52].

Z-$L1_0$(001)[001] || MgO(001)[001]

X-$L1_0$(100)[010] || MgO(001)[010] (1)

Y-$L1_0$(100)[001] || MgO(001)[010]

It was initially assumed that the migration of the Pt atoms into the fcc-Co (001) epitaxial layer during the reaction would cause the synthesis of only one Z-variant in $L1_0$-$Pt_{50}Co_{50}$ films. This should have a high PMA constant $K_u = K_1(L1_0) - 2\pi M_S^2 \sim 3.7 \times 10^7$ erg/cm$^3$ and in case of uniform magnetization rotation should have high coercivity $H_C \sim 2K_u/M_S = 92$ kOe, where $K_1(L1_0) = 4.1 \times 10^7$ erg/cm$^3$ is the first constant of magnetocrystalline anisotropy and $M_S = 800$ emu/cm$^3$ is the saturation magnetization for bulk $L1_0$-$Pt_{50}Co_{50}$ [53]. In contrast to this, after annealing at 600 °C the intensity ratio I(200)/I(002) is ~2, which corresponds with ordered $L1_0$ with near equal volume fractions of the X-,Y-, Z-variants. The average crystallite size of the $L1_0$Co50Pt50 was determined from the (001) peaks using the Scherrer equation after annealing in 400–700 °C temperature interval at approximately 8–10 nm. The total disappearance of the (001)$L1_0$ and (002)$L1_0$ peaks above 750 °C indicated the $L1_0 \rightarrow$ A1 transition. The (002)A1 reflection grew after annealing at 850 °C, which denotes the formation of the high crystalline quality epitaxial A1-$Co_{50}Pt_{50}$(001) layer that has the lattice parameter 0.3764 nm and a simple cube-on-cube orientation relationship with the MgO(001) substrate [26]. It is important to note that the A1 phase began to form at 750 °C, which is less than 825 °C of bulk samples. An explanation for this difference may be related to a decrease in the order-disorder transition temperature with decreasing size nanoparticles [1]. For instance, Alloyeau et al. found that the transition temperatures for 2.4–3 nm CoPt nanoparticles to be 325-175 °C lower than the bulk material [54]. This suggested that $L1_0$Co50Pt50 films consisting of 8–10 nm crystallites have a lower transition temperature than the bulk samples. Thus, an analysis of the X-ray diffraction results showed the phase sequence formation (2)

50Pt/50fcc-Co(001) → 400 °C $L1_0$ → 750 °C A1-$Pt_{50}Co_{50}$ (2)

Fig. 1b shows the in-plane torque curves $L_{||}(\phi)$ of the 50Pt/50fcc-Co(001) bilayer at different annealing temperatures. The dependences $L_{||}^{rot}(T_a)$ and $K_4(T_a)$ as functions of the annealing temperature $T_a$ were calculated from torque curves $L_{||}(\phi)$ and summarized in Fig. 1c. The $K_4$ constant did not change beyond 400 °C and this is confirmed by the absence of the structural transformations in the fcc-Co(001) layer. Above 400 °C, the $K_4$ value began to slightly decrease due to the start of the synthesis of the low crystalline quality epitaxial $L1_0$(001) layer. It is important to note that the initial defective $L1_0$(001) thin layer had close to zero anisotropy in the temperature range of 400–550 °C and therefore does not contribute to the $K_4$ constant but only reduces insignificantly the thickness of the reactive fcc-Co(001) layer. After annealing above 550 °C, the $K_4$ value rose sharply and reached the maximum value $K_4 = -11 \times 10^5$ erg/cm$^3$ at 700 °C, which indicated an increase in the thickness and crystalline quality of the epitaxial $L1_0$(001) layer. In the temperature range of 550–750 °C for large angles $\phi$, the in-plane torque curves $L_{||}(\phi)$ and the four-fold anisotropy ½$K_4$Sin4$\phi$ contained the $L_{||}^{rot}$ contribution from RMA $L_{|}(\phi) = \pm L_{||}^{rot} + ½K_4$ Sin4$\phi$ (Fig. 1b). The constant $L_{||}^{rot}$ began to grow very slowly above 400 °C and reached the maximum value $L_{||}^{rot} = 8.0 \times 10^5$ erg/cm$^3$ at 600 °C and 700 °C. After annealing at 750 °C, the constant $L_{||}^{rot}$ decreased to zero and the $K_4$ value decreased to $K_4 - 5.5 \times 10^5$ erg/cm$^3$. An analysis of the dependence of $K_4(T_a)$ and the X-ray diffraction patterns after annealing at 750 °C showed that the first constant of magnetocrystalline anisotropy $K_1$(A1-$Co_{50}Pt_{50}$) of the disordered A1-$Co_{50}Pt_{50}$ phase is equal to the four-fold anisotropy constant $K_4$ (850 °C) = $K_1$(A1-$Co_{50}Pt_{50}$) = $-5.5 \times 10^5$ erg/cm$^3$. This value is close to the bulk sample value of the disordered cubic $Pt_{52}Co_{48} \approx -6 \cdot 10^5$ erg/cm$^3$ [55]. In summary, the analysis of the X-ray diffraction patterns and the magnetic studies showed that RMA and the $L1_0$ phase existed together in the temperature range of 400–750 °C, which suggested that the nature of RMA is related to the structure of the $L1_0$ film.

Fig. 2 illustrates the in-plane torque clockwise curves for the $L1_0$ film after annealing at 600 °C with RMA, in which the easy axis (ea) is aligned along the [100] (curve1) and [110] (curve 2) directions. The curves coincided, within experimental accuracy, after a shift to an angle of ~ 45°, which is equal to the angle between the [100] and [110] directions. This clearly demonstrates that, unlike RMA, the easy axes of the four-fold anisotropy do not rotate beyond the magnetic field direction, but tightly bound to the [110] and [1-10] directions of the $L1_0$(001) film and the MgO (001) substrate (Fig. 3). Therefore, it is reasonable to assume that $L1_0$ films conditionally consist of two layers after annealing at 600 °C. The first $L1_0$(001) layer is an epitaxially intergrown layer with the MgO (001) substrate (EILWS-layer) and is not subject to structural changes under the influence of a magnetic field. The second layer is a surface RMA-layer, in which $L1_0$ crystallites tend to line up in a direction close to the direction of the magnetic field (Fig. 3). If the $L1_0$ crystallites are aligned by c-axis in one direction then they must have an anisotropy constant equal to $K_1(L1_0) = 4.1 \times 10^7$ erg/cm$^3$ [53], however experiments showed RMA with a constant $L_{||}^{rot} = 8.0 \times 10^5$ erg/cm$^3$. Under this assumption, the ratio $L_{||}^{rot}/K_1(L1_0) \sim 1.5\%$, means that only an insignificant part of the $L1_0$ film participates in the RMA process. This suggests that RMA is a magnetostructural surface phenomenon. Fig. 4a represents the in-plane and out-of-plane hysteresis loops of the 50Pt/50fcc-Co(001) thin film after annealing at 600 °C, obtained along the [110] (in-plane) and [001] (out-of-plane) directions, respectively (Fig. 3). The out-of-plane hysteresis loop had a significant slope compared to the in-plane hysteresis loop, which is associated with the presence of a two-fold shape anisotropy. Fig. 4b showed the out-of-plane magnetic torque curve $L\perp(\phi)$, was obtained by rotating the magnetic field from the [110] (in-plane) direction via [001] (out-of-plane) to the [1-10] (in-plane) direction. The $L\perp(\phi)$ contains a main contribution from two-fold perpendicular anisotropy with an easy axis lying in the film plane, a constant $K_u = 1.1 \times 10^6$ erg/cm$^3$ and a contribution from RMA with a constant $L\perp^{rot} = 8.0 \times 10^5$ erg/cm$^3$. It should be noted that the equality

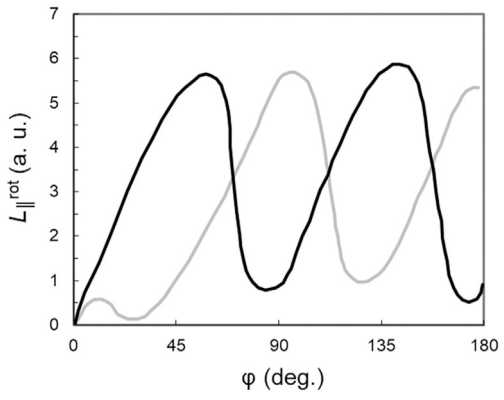


**Fig. 2.** The in-plane torque clockwise curves for the RMA $L1_0$-$Co_{50}Pt_{50}$ film in which the easy axes were lined up along the [110] (curve 1) and [100] (curve 2) directions of the MgO(001) substrate. Since these curves do not match, this means that the easy axes of four-fold anisotropy coincide with the [110] and [1-10] directions of the MgO(001) substrate and do not change their directions under the influence of a magnetic field.

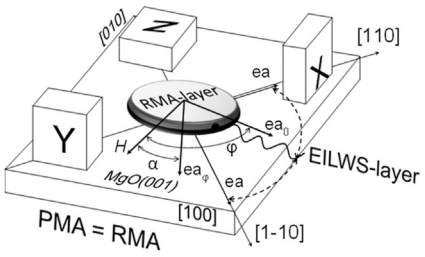


**Fig. 3.** Schematic view of the three X-, Y-, Z-variants of $L1_0$ growing on the (001) surface of MgO. The $L1_0$ structure consists of two layers: the epitaxially intergrown layer with a MgO(001) substrate (EILWS-layer) having classical fourfold anisotropy with an easy axis (ea) lying along the [110] and [1-10] directions of MgO(001) and a surface RMA-layer possessing a rotating easy axis under the influence of a magnetic field. In the RMA-layer the original easy axis $ea_0$ lies along the magnetic field direction. When the magnetic field is rotates by an angle $\phi$ the easy axis shifts to the $ea_\phi$ magnetic field direction but lags by an angle $\alpha$.

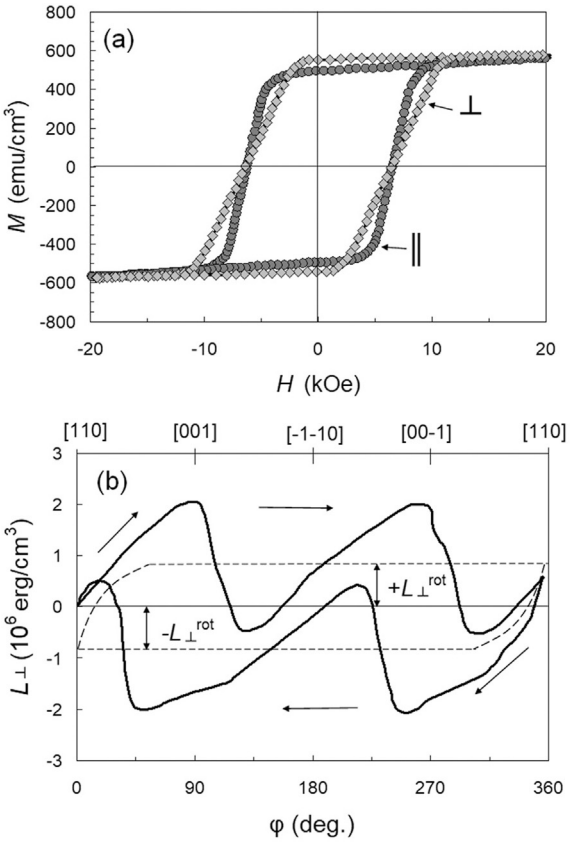


**Fig. 4.** In-plane and out-of-plane hysteresis loops (a) and out-of-plane torque curve $L\perp(\phi)$ (b). The equalities of the out-of-plane and in-plane $H_c^{||} = H_c\perp$ coercivities and the in-plane and out-of-plane $L_{||}^{rot} = L\perp^{rot}$ constants are associated with RMA spatial uniformity. The torque curve $L\perp(\phi)$ contains out-of-plane twofold anisotropy, which is determined by the form anisotropy of the EILWS-layer (Fig. 3).

$L^{rot} = L\perp^{rot} = L_{||}^{rot} = 8.0 \times 10^5$ erg/cm$^3$ and the equality of the in-plane and out-of-plane coercive forces $H_{||} = H\perp \sim 6$ kOe indicated the spatial isotropy of the RMA phenomena, which was discovered earlier in $L1_0$CoPt(111) [12], $L1_0$FePt [13] and MnBi [16] thin films. In addition, the slightly distorted torque curve shape indicates the presence of four-fold anisotropy. In-plane perpendicular anisotropy is given by $K_u = 2\pi M_S^2 \pm \Delta K$ and contains the anisotropy shape $2\pi M_S^2$ and the anomalous part of the perpendicular anisotropy $\pm \Delta K$, which does not exceed 50% of $2\pi M_S^2$ for many in-plane films. For simplicity, neglecting $\Delta K$, the rough value of magnetization is ~ 280 emu/cm$^3$, which is less than the magnetization ~ 500 emu/cm$^3$ of this sample and significantly less than the bulk value 800 emu/cm$^3$ [53]. From this, it follows that in-plane perpendicular anisotropy is associated with the EILWS-layer, which is an only part of the $L1_0$ layer. The above data (Figs. 3 and 4) only indicated the existence of a bilayer structure in the $L1_0$ film but does not give the opportunity to determine the exact ratio of thicknesses between the surface RMA-layer and the EILWS-layer. This makes it impossible to find the exact values of the constants $K_4$, $K_u$, $L^{rot}$. In summary, after annealing at 600 °C, the $L1_0$ films contain an EILWS-layer having a four-fold anisotropy constant $K_4 > -7.8 \times 10^5$ erg/cm$^3$ with easy [110] and [1-10] axes and an in-plane perpendicular anisotropy $K_u > 1.1 \times 10^6$ erg/cm$^3$, which is exchanged coupled with a surface RMA-layer having $L^{rot} > 8.0 \times 10^5$ erg/cm$^3$ (Fig. 3). It is important to note that the surface nature of the RMA phenomena is consistent with the well-known fact that RMA phenomena was only found in thin films and never in bulk samples. It was shown in Ref. [26] that if the set of X-, Y-, Z variants are exchanged coupled and their equal volume fractions, then the magnetic anisotropy is described by cubic anisotropy with easy axes (ea) coinciding with the [110] and [1-10] directions of the film and MgO (001) substrate (Fig. 3) and having a constant $K_4 = 2/3\ K_2(L1_0)$, where $K_2(L1_0)$ is the second magnetocrystalline anisotropy constant of the $L1_0$-$Pt_{50}Co_{50}$. Hence the value of $K_2(L1_0) > -1.7 \times 10^6$ erg/cm$^3$, which is more than an order of magnitude is smaller than the first magnetocrystalline anisotropy constant $K_1(L1_0) = 4.1 \times 10^7$ erg/cm$^3$. It is important to keep in mind that the c-axes of the three $L1_0$ variants are mutually perpendicular to each other and therefore the uniaxial anisotropies with constants $K_1$ of the X-, Y-, Z-variants do not contribute to the cubic anisotropy. This suggested that the EILWS-layer with the constant $K_4 > -7.8 \times 10^5$ erg/cm$^3$ is a soft magnetic layer. In contrast, to the EILWS-layer, the surface RMA-layer is a hard-magnetic layer and is consistent with the magnetic studies of polycrystalline RMA-films having a coercivity of several kiloersted [12,13,15,16].

Finally, we did not find any evidence of out-of-plane uniaxial PMA, and therefore our finding proves that the hard-magnetic properties of the $L1_0$-$Pt_{50}Co_{50}$ films are linked to the RMA-layer.

### 3.2. Phase transformations and magnetic properties in 32Pt/68fcc-Co(001) thin films

Like 50Pt/50fcc-Co (001) bilayers, X-ray diffraction patterns of the 32Pt/68fcc-Co (001) bilayers showed that the $L1_0$ starts at 400 °C, which then turns into a disordered A1-$Pt_{32}Co_{68}$ phase at 550 °C (Fig. 5a). The extremely broad and low (001), (002), and (200) reflections from $L1_0$ suggested that only a thin low crystalline quality $L1_0$-$Pt_{50}Co_{50}$ layer of equiatomic composition starts on the Pt/Co interface, which is then transformed to the disordered $A_1$-$Pt_{32}Co_{68}$ phase following the solid-state reaction of $L1_0$-$Pt_{50}Co_{50}$ with a residual fcc-Co (001) layer ($L1_0$-$Pt_{50}Co_{50}$ + fcc-Co → (550 °C) A1-$Pt_{32}Co_{68}$). The lattice parameter a = 0.3700 nm of the disordered A1-$Pt_{32}Co_{68}$ phase after annealing at 850 °C was determined using the (200) reflection. Thus, the X-ray diffraction results showed the phase sequence formation (3)

$$32Pt/68fcc\text{-}Co(001) \rightarrow 400\ ^\circ C\ L1_0 \rightarrow 600\ ^\circ C\ A1\text{-}Pt_{32}Co_{68} \quad (3)$$

Fig. 5b represents the temperature dependence of the in-plane four-fold anisotropy constant $K_4(T_a)$. The independence of $K_4$ ($T_a$) from the annealing temperature up to 400 °C is consistent with the data from X-ray diffraction, which indicated the absence of mixing and reaction between the Pt and Co. layers. A slight decrease of $K_4(T_a)$ in 50Pt/50fcc-Co(001) films in the temperature range of

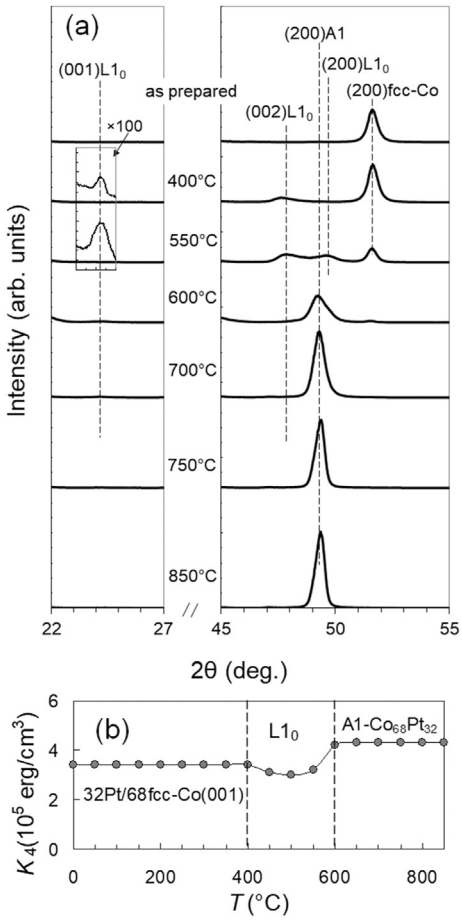


**Fig. 5.** X-ray diffraction patterns (a) and the dependence of the four-fold anisotropy constant $K_4(T_a)$ on the annealing temperature (b) showing the sequential synthesis of $L1_0$ and A1-$Co_{68}Pt_{32}$ in epitaxial 32Pt/68Co(001) thin films under annealing temperatures from room temperature up to 850 °C.

400–550 °C confirms the formation of a low crystalline quality very thin $L1_0$ layer. It is interesting to note that the initial $L1_0$(001) layer formed on the Pt/fcc-Co(001) interface does not have four-fold magnetic anisotropy since the $K_4(T_a)$ dependence decreases, not increasing above 400 °C (Figs. 1c and 5b). The decrease of the $K_4(T_a)$ constant above 400 °C is a consequence of the formation of the defective $L1_0$ (001) layer with a thickness of ~ 20–25 nm, which reduces the thickness of the fcc-Co(001) layer by ~ 10–12%. The real mechanisms of the lack of four-fold magnetic anisotropy is not clear and additional structural studies is necessary to understand the initial stage of $L1_0$(001) synthesis. In the temperature range of 400–600 °C, the 32Pt/68fccCo (001) thin films contained the defective $L1_0$-$Pt_{50}Co_{50}$ and Co(001) layers, which did not possess RMA and therefore had the typical in-plane hysteresis loops showing small coercive force about 300 Oe. Above 550 °C the defective $L1_0$(001) layer grew into a high-quality disordered A1-$Pt_{32}Co_{68}$(001) layer with the first magnetic anisotropy constant $K_1$(A1-$Pt_{32}Co_{68}$) = $K_4$(850 °C) = - 4.3 × 10$^5$ erg/cm$^3$.

The literature review shows the presence of metastable $D0_{19}$-$Co_3Pt$ [3] and $L1_2$- $Co_3Pt$ [56] phases in the Co-rich side of phase diagram Co-Pt. The new modified Co-Pt phase diagram contains $Co_3Pt$ in the Pt32Co68 samples [57]. However, our results do not suggest the formation of $Co_3Pt$ in 32Pt/68fccCo(001) films after annealing up to 850 °C. Therefore, further study of phase formation in solid-state reactions in the 100-68 at. % range of Co, especially in 25Pt/75Co films, are needed to clarify the Co-rich side of the Co-Pt phase diagram.

## 4. Discussion

### 4.1. Reaction mechanism in Pt/Co bilayers and prediction of the phase transition at 400 °C

For most metals with high melting points $T_m$, the diffusion coefficient $D << 10^{-24}$ cm$^2$/s is below 400 °C. Taking into account the typical annealing time of 1 h, this corresponds to a nearly zero diffusion length $l = (Dt)^{1/2} = 0.001$ nm, which is insufficient for the formation of the CoPt phase. This is in accordance with Tamann's empirical law, according to which there is no bulk diffusion below $0.5T_m$ (for Pt/Co bilayers $0.5T_m$ > 750 °C). In contrast to the generally accepted diffusion mechanism, we are developing an alternative mechanism for low-temperature solid-state reactions [36–50,58]. The basic concepts include: an initiation temperature $T_{in}$ < 400 °C, no mixing at the Pt/Co interface and no reaction initiated between the Co and Pt. When the temperature increases above the initiation temperature $T_{in}$ > 400 °C, strong attractive chemical interactions arise between the Co and Pt atoms. This destroys the old chemical bonds between the atoms in one of the reactants (Co or Pt), causing these atoms to migrate into the layer of the second reactant (Pt or Co) and form the first $L1_0$-CoPt phase. In particular, the chemical interactions create rapid atomic migration during the reaction and hence increase the "effective diffusion coefficient" by 12–18 orders of magnitude. It is important to note that when the temperature changes around $T_{in}$ = 400 °C, the same chemical interactions initiate a phase transition in the synthesized $L1_0$-CoPt phase.

The above results and work [26] reveals that the $L1_0$ is the first phase which forms on the Co/Pt interface at the initiation temperature $T_{in}$ ~ 400 °C in a broad composition range between 32% and 72% of Pt. Our approach predicts the existence of a phase transition at ~ 400 °C in the 32–72% Pt composition region, which is absent in the Co-Pt bulk phase diagram. Since the reaction between Co and Pt led to the synthesis of the ordered $L1_0$ phase, this suggested that the phase transition at a temperature of ~ 400 °C should be related to the ordering peculiarities in the $L1_0$. However, a literature review showed that around 400 °C Co clustering or phase separation into Pt-rich and Co-rich regions is observed in $Co_xPt_{1-x}$ thin film alloys [4,11,59–63], which occurred via spinodal decomposition [63]. It follows from this that the structural origin of the phase transformation at 400 °C remains unclear and needs to be further investigated.

### 4.2. RMA model

We hypothesized that the RMA phenomena of the surface layer in $L1_0$-$Pt_{50}Co_{50}$ films is as a result of the field-induced rearrangements of the tetragonal X-,Y-, Z-variants by twining. Typically, the close-packed planes are twin planes and the {111} planes are twin planes of the $L1_0$ cell. When the $L1_0$-$Pt_{50}Co_{50}$ film is placed into a magnetic field nanotwins with an easy c-axis around the direction of the magnetic field arises in the X-,Y-, Z-variants of the surface layer and created an effective easy axis. The real picture can get very complicated because of the formation of nanotwins with different spatial orientations which formed a complex twin structure. When the magnetic field rotates, the twin structure is rearranged, leading to the rotation of the effective easy axis following the direction of the magnetic field. It is important to note that the c-axis of the nanotwins does not line up strictly in the magnetic field direction and can form large angles, so the effective easy axis always has a lag angle $\alpha$ to the magnetic field direction (Fig. 3). The represented RMA model originates from the explanation of large magnetic-

field-induced strains (MFIS) and the ferromagnetic shape-memory (FSM) effect observed in Heusler alloys. The origin of MFIS is explained by the high mobility of the twin boundary as a result of an external magnetic field, which generates a rearrangement of martensitic variants without changing phase [64–68]. The mechanism behind the magnetic shape-memory effect is associated with the formation of martensitic twins whose c-axes are oriented around the applied magnetic field and can exhibit MFIS up to 12% [64–69]. The investigated samples exhibited MFIS and contains three martensitic modifications: five-layered modulated tetragonal martensite (10 M) (c/a <1), seven-layered modulation (14 M) with an orthorhombic lattice and non-modulated martensite (NM) with an $L1_0$ tetragonal lattice (c/a >1). It is important to note that the tetragonal martensite 10 M, like $L1_0$-CoPt, has three martensite X-, Y-, Z-variants (Fig. 3), however, unlike $L1_0$-CoPt, the twin boundary of 10 M is the {101} plane [70]. The general nature of RMA and MFIS is confirmed by the reversible reorientation of the easy magnetization direction under an applied magnetic field in single-crystal samples of near-stoichiometric $Ni_2MnGa$ alloys [65,71]. Also, more indirect evidence is the approximate equality of the in-plane and out-of-plane hysteresis loops [72–79], which is a characteristic of spatial isotropy of RMA in thin films [12,13,15,16]. Like the $L1_0$ of our work (Fig. 4a), the shape mismatch in the Ni-Mn-Ga thin film hysteresis loops is caused by the four-fold anisotropy and shape anisotropy of the film sample. However, subtracting the demagnetizing field from the out-of-plane hysteresis loop led to a good equality with the in-plane loop [79]. In addition, RMA was observed in polycrystalline $(Co_2Fe)_xGe_{1-x}$ Heusler alloy films, which had similar in-plane and out-of-plane angular hysteresis loops [80]. Summarizing the above, we not only justified the general nature of RMA and MFIS, we can also assume the existence of the RMA phenomena in ferromagnetic MFIS-Heusler alloy films.

## 5. Conclusions

Three variants of the ordered $L1_0$ phase grew above 400 °C in 50Pt/50fcc-Co (001) thin films and possessed rotatable magnetic anisotropy. Torque measurements revealed that the $L1_0$ films contained a soft magnetic layer epitaxially intergrown with the MgO(001) substrate and a top layer having rotatable magnetic anisotropy. The general nature of rotatable magnetic anisotropy and magnetic-field-induced strains in Heusler alloys is substantiated. Above 750 °C the $L1_0$ turns into disordered A1-$Co_{50}Pt_{50}$ having the first magnetocrystalline anisotropy constant $K_1 = -5.5 \times 10^5$ erg/cm$^3$. In 32Pt/68fcc-Co (001) thin films above 400 °C do not show the rotatable magnetic anisotropy because a very thin defective $L1_0$ layer was ~~is~~ formed. Above 550 °C defective $L1_0$ layer reacts with a residual fcc-Co (001) layer and forms the disordered A1-$Co_{68}Pt_{32}$ alloys film with a magnetic anisotropy constant $K_1$(A1-$Co_{68}Pt_{32}$) = - 4.3 × $10^5$ erg/cm$^3$. The second magnetocrystalline anisotropy constant of the ordered $L1_0$-$Co_{50}Pt_{50}$ phase is defined as $K_2$($L1_0$-$Co_{50}Pt_{50}$) > - 1.2 × $10^6$ erg/cm$^3$. Our findings revealed not only the surface character of rotatable magnetic anisotropy but also its vital role in the perpendicular anisotropy of hard magnetic $L1_0$ films.

## CRediT authorship contribution statement

**V.G. Myagkov:** Conceptualization, Supervision, Funding acquisition, Writing - review & editing. **L.E. Bykova:** Investigation, Visualization, Funding acquisition. **V.S. Zhigalov:** Investigation, Formal analysis, Funding acquisition. **A.A. Matsynin:** Investigation, Formal analysis, Visualization. **D.A. Velikanov:** Investigation, Methodology. **G.N. Bondarenko:** Investigation, Methodology.

## Declaration of competing interest

The authors declare that they have no known competing financial interests or personal relationships that could have appeared to influence the work reported in this paper.

## Acknowledgements

This study was supported by the Russian Foundation for Basic Research, Government of Krasnoyarsk Territory, Krasnoyarsk Regional Fund of Science for the research projects no. 19-43-240003. The authors thank I.V. Nemtsev for assisting with the measurements of the samples' composition. The work is partially based upon the experiments performed at Krasnoyarsk Regional Center of Research Equipment of Federal Research Center « Krasnoyarsk Science Center SB RAS».

## Appendix A. Supplementary data

Supplementary data to this article can be found online at https://doi.org/10.1016/j.jallcom.2020.157938.

## References

[1] P. Andreazza, V. Pierron-Bohnes, F. Tournus, C. Andreazza-Vignollea, V. Dupuis, Structure and order in cobalt/platinum-type nanoalloys: from thin films to supported clusters, Surf. Sci. Rep. 70 (2015) 188–258, https://doi.org/10.1016/j.surfrep.2015.02.002.
[2] D. Weller, A. Moser, L. Folks, M.E. Best, W. Lee, M.F. Toney, M. Schwickert, J.-U. Thiele, M.F. Doerner, High $K_u$ materials approach to 100 Gbits/in$^2$, IEEE Trans. Magn. 36 (2000) 10–15, https://doi.org/10.1109/20.824418.
[3] M. Ohtake, D. Suzuki, M. Futamoto, Characterization of metastable crystal structure for Co-Pt alloy thin film by x-ray diffraction, J. Appl. Phys. 115 (2014), 17C116-1 - 17C116-3, https://doi: 10.1063/1.4864139.
[4] J.O. Cross, M. Newville, B.B. Maranville, C. Bordel, F. Hellman, V.G. Harris, Evidence for nanoscale two-dimensional Co clusters in $CoPt_3$ films with perpendicular magnetic anisotropy, J. Phys. Condens. Matter 22 (2010), https://doi.org/10.1088/0953-8984/22/14/146002, 146002-1 – 146002-7.
[5] Y.-S. Chen, H.-Y. Dai, Y.-W. Hsu, S.-L. Ou, S.-W. Chen, H.-C. Lu, S.-F. Wang, A.-C. Sun, Room temperature deposition of perpendicular magnetic anisotropic Co3Pt thin films on glass substrate, J. Magn. Magn Mater. 425 (2017) 57–62, https://doi.org/10.1016/j.jmmm.2016.10.117.
[6] D. Makarov, E. Bermúdez-Ureña, O.G. Schmidt, F. Liscio, M. Maret, C. Brombacher, S. Schulze, M. Hietschold, M. Albrecht, Nanopatterned CoPt alloys with perpendicular magnetic anisotropy, Appl. Phys. Lett. 93 (2008), https://doi.org/10.1063/1.2993334, 153112-1 - 153112-3.
[7] P. Caesario, T. Harumoto, Y. Nakamura, J. Shi, Strong perpendicular magnetic anisotropy induced by broken symmetry of A1-CoPt, J. Appl. Phys. 125 (2019), https://doi.org/10.1063/1.5081747, 053904-1 - 053904-5.
[8] A.I. Figueroa, J. Bartolomé, L.M. García, F. Bartolomé, O. Bunău, J. Stankiewicz, L. Ruiz, J.M. González-Calbet, F. Petroff, C. Deranlot, S. Pascarelli, P. Bencok, N.B. Brookes, F. Wilhelm, A. Smekhova, A. Rogalev, Structural and magnetic properties of granular Co-Pt multilayers with perpendicular magnetic anisotropy, Phys. Rev. B 90 (2014), https://doi.org/10.1103/PhysRevB.90.174421, 174421-1 - 174421-16.
[9] C.H. Su, 1.S.C Lo, J. van Lierop, K.W. Lin, H. Ouyang, The intermixing induced perpendicular magnetic anisotropy in ultrathin Co/Pt multilayers, J. Appl. Phys. 105 (2009), https://doi.org/10.1063/1.3070639, 07C316-1 - 07C316-3.
[10] H. Ouyang, Y.-H. Han, S.-C. Lo, C.-H. Su, Y.-R. Shiu, K.-W. Lin, R.D. Desautels, J. van Lierop, Tailoring perpendicular magnetic anisotropy in ultrathin Co/Pt multilayers coupled to NiO, Phys. Rev. B 81 (2010), https://doi.org/10.1103/PhysRevB.81.224412, 224412-1 - 224412-7.
[11] S.-E. Park, P.-Y. Jung, K.-B. Kim, Magnetic properties and microstructural analysis of sputter deposited and annealed Co-Pt alloys, J. Appl. Phys. 77 (1995) 2641–2647, https://doi.org/10.1063/1.358730.
[12] V.G. Myagkov, V.S. Zhigalov, L.E. Bykova, G.N. Bondarenko, A.N. Rybakova, A.A. Matsynin, I.A. Tambasov, M.N. Volochaev, D.A. Velikanov, High magnetic rotatable anisotropy in epitaxial $L1_0$CoPt(111) thin films, JETP Lett. (Engl. Transl.) 6 (2015) 355–360, https://doi.org/10.1134/S002364015180101.
[13] V.S. Zhigalov, V.G. Myagkov, L.E. Bykova, G.N. Bondarenko, D.A. Velikanov, M.N. Volochaev, Rotational magnetic anisotropy in polycrystalline FePt films fabricated by solid-state synthesis, Phys. Solid State 60 (2018) 178–182, https://doi.org/10.1134/S1063783418010298.
[14] M.J. O'Shea, K.M. Lee, A. Fert, The magnetic state and its macroscopic anisotropy in amorphous rare-earth alloys (invited), J. Appl. Phys. 67 (1990), https://doi.org/10.1063/1.345959, 5769-1574.
[15] V.G. Myagkov, V.S. Zhigalov, L.E. Bykova, G.N. Bondarenko, Yu L. Mikhlin,

G.S. Patrin, D.A. Velikanov, Solid-state formation of ferromagnetic δ-$Mn_{0.6}Ga_{0.4}$ thin films with high rotatable uniaxial anisotropy, Phys. Status Solidi B 249 (2012), https://doi.org/10.1002/pssb.201248064, 1541-154.
[16] V.G. Myagkov, L.E. Bykova, V. Yu Yakovchuk, A.A. Matsynin, D.A. Velikanov, G.S. Patrin, G. Yu Yurkin, G.N. Bondarenko, High rotatable magnetic anisotropy in MnBi thin films, JETP Lett. (Engl. Transl.) 105 (2017) 651–656, https://doi.org/10.1134/S0021364017100095.
[17] S. Tacchi, S. Fin, G. Carlotti, G. Gubbiotti, M. Madami, M. Barturen, M. Marangolo, M. Eddrief, D. Bisero, A. Rettori, M.G. Pini, Rotatable magnetic anisotropy in a Fe0.8Ga0.2 thin film with stripe domains: dynamics versus statics, Phys. Rev. B 89 (2014), https://doi.org/10.1103/PhysRevB.89.024411, 024411-1 - 024411-6.
[18] W.T. Soh, N.N. Phuoc, C.Y. Tan, C.K. Ong, Magnetization dynamics in permalloy films with stripe domains, J. Appl. Phys. 114 (2013), https://doi.org/10.1063/1.4817767, 053908-1 - 053908-7.
[19] G. Chai, N.N. Phuoc, C.K. Ong, Exchange coupling driven omnidirectional rotatable anisotropy in ferrite doped CoFe thin film, Sci. Rep. 2 (2012) 832, https://doi.org/10.1038/srep00832, 1-5.
[20] L.-C. Garnier, M. Marangolo, M. Eddrief, D. Bisero, S. Fin, F. Casoli, M.G. Pini, A. Rettori, S. Tacchi, Stripe domains reorientation in ferromagnetic films with perpendicular magnetic anisotropy, J. Phys. Mater. 3 (2020), https://doi.org/10.1088/2515-7639/ab6ea5, 024001-1 – 024001-25.
[21] N. Yasui, A. Imada, T. Den, Electrodeposition of (001) oriented $CoPtL1_0$ columns into anodic alumina films, Appl. Phys. Lett. 83 (2003) 3347–3349, https://doi.org/10.1063/1.1622787.
[22] Y.S. Chen, A.-C. Sun, H.Y. Lee, H.-C. Lu, S.-F. Wang, P. Sharma, Enhanced coercivity of HCP Co–Pt alloy thin films on a glass substrate at room temperature for patterned media, J. Magn. Magn Mater. 391 (2015) 12–16, https://doi.org/10.1016/j.jmmm.2015.04.080.
[23] Y. Xu, Z.G. Sun, Y. Qiang, D.J. Sellmyer, Preparation and magnetic properties of CoPt and CoPt:Ag nanocluster films, J. Magn. Magn Mater. 266 (2003) 164–170, https://doi.org/10.1016/S0304-8853(03)00467-0.
[24] S.P. Withrow, C.W. White, J.D. Budai, L.A. Boatner, K.D. Sorge, J.R. Thompson, R. Kalyanaraman, Ion beam synthesis of magnetic Co–Pt alloys in Al2O3, J. Magn. Magn Mater. 260 (2003) 319–329, https://doi.org/10.1016/S0304-8853(02)01322-7.
[25] F.-T. Yuan, A.-C. Sun, C.F. Huang, J.-H. Hsu, Intra-grain perpendicular percolated $L1_1$ CoPt thin films, Nanotechnology 25 (2014), https://doi.org/10.1088/0957-4484/25/16/165601, 165601-1 - 165601-6.
[26] V.G. Myagkov, L.E. Bykova, V.S. Zhigalov, A.A. Matsynin, D.A. Velikanov, G.N. Bondarenko, Phase formation sequence, magnetic and structural development during solid-state reactions in epitaxial 72Pt/28fcc-Co(001) thin films, J. Alloys Compd. 706 (2017) 447–454, https://doi.org/10.1016/j.jallcom.2017.02.261.
[27] F. Si Abdallaha, S.M. Chérif b, Kh Bouamamaa, Y. Roussigné b, J.-H. Hsu, Effect of deposition temperature on morphological, magnetic and elastic properties of ultrathin Co49Pt51 films, Appl. Surf. Sci. 433 (2018) 647–652, https://doi.org/10.1016/j.apsusc.2017.10.005.
[28] F.T. Yuan, H.W. Chang, P.Y. Lee, C.Y. Chang, C. C Chi, H. Ouyang, Perpendicular magnetic anisotropy of non-epitaxial hexagonal Co50Pt50 thin films prepared at room temperature, J. Alloys Compd. 628 (2015) 263–266, https://doi.org/10.1016/j.jallcom.2014.12.198.
[29] H. An, J. Wang, J. Szivos, T. Harumoto, T. Sannomiya, S. Muraishi, G. Safran, Y. Nakamura, J. Shi, Perpendicular coercivity enhancement of CoPt/TiN films by nitrogen incorporation during deposition, J. Appl. Phys. 118 (2015), https://doi.org/10.1063/1.4936365, 203907-1 - 203907- 4.
[30] Z.Y. Pan, R.S. Rawat, J.J. Lin, S. Mahmood, R.V. Ramanujan, P. Lee, S.V. Springham, T.L. Tan, Oriented growth of CoPt nanoparticles by pulsed laser deposition, Appl. Phys. A 101 (2010) 609–613, https://doi.org/10.1007/s00339-010-5937-0.
[31] J.M. Poate, K.N. Tu, J.W. Mayer (Eds.), Thin Films-Interdiffusion and Reaction, Willey-Interscience, New York, 1978, p. 578.
[32] R. Pretorius, C.C. Theron, A. Vantomme, J.W. Mayer, Compound phase formation in thin film structures, Crit. Rev. Solid State Mater. Sci. 24 (1999) 1–62, https://doi.org/10.1080/10408439991329161.
[33] J.J. Hoyt, L.N. Brush, On the nucleation of an intermediate phase at an interface in the presence of a concentration gradient, J. Appl. Phys. 78 (1995) 1589–1594, https://doi.org/10.1063/1.360252.
[34] L.A. Clevenger, L.A. Clevenger, B. Arcot, W. Ziegler, E.G. Colgan, Q.Z. Hong, F.M. d'Heurle, C. Cabral Jr., T.A. Gallo, J.M.E. Harper, Interdiffusion and phase formation in Cu(Sn) alloy films, J. Appl. Phys. 83 (1998) 90–99, https://doi.org/10.1063/1.366728.
[35] V.G. Myagkov, L.E. Bykova, V.S. Zhigalov, A.I. Pol'skii, F.V. Myagkov, Solid-phase reactions, self-propagating high-temperature synthesis, and order-disorder phase transition in thin films, JETP Lett. (Engl. Transl.) 71 (2000) 183–186, https://doi.org/10.1134/1.568310.
[36] V.G. Myagkov, Yu L. Mikhlin, L.E. Bykova, V.K. Mal'tsev, G.N. Bondarenko, Long-range chemical interaction in solid-state synthesis: the Formation of a CuAu alloy in Au/β-Co(001)/Cu(001) epitaxial film structures, JETP Lett. (Engl. Transl.) 90 (2009) 111–115, https://doi.org/10.1134/S0021364009140069.
[37] V.G. Myagkov, V.S. Zhigalov, L.E. Bykova, G.N. Bondarenko, Solid-state synthesis and phase transformations in Ni/Fe films: structural and magnetic studies, J. Magn. Magn Mater. 305 (2006) 534–545, https://doi.org/10.1016/j.jmmm.2006.02.265.
[38] V.G. Myagkov, V.S. Zhigalov, L.E. Bykova, G.N. Bondarenko, Long-range chemical interaction in solid-state synthesis: chemical interaction between Ni and Fe in epitaxial Ni(001)/Ag(001)/Fe(001) trilayers", Int. J. SHS 18 (2) (2009) 117–124, https://doi.org/10.3103/S1061386209020095" title="10.3103/S1061386209020095">10.3103/S1061386209020095.
[39] V.G. Myagkov, L.E. Bykova, S.M. Zharkov, G.N. Bondarenko, Formation of NiAl shape memory alloy thin films by a solid-state reaction, Solid State Phenom. 138 (2008) 377–384. https://doi.org/10.4028/www.scientific.net/SSP.138.377.
[40] V.G. Myagkov, L.E. Bykova, L.A. Li, I.A. Turpanov, G.N. Bondarenko, Solid-phase reactions, self-propagating high-temperature synthesis, and martensitic transformations in thin films, Dokl. Phys. 47 (2002) 95–98, https://doi.org/10.1134/1.1462075.
[41] V.G. Myagkov, Yu L. Mikhlin, L.E. Bykova, G.V. Bondarenko, G.N. Bondarenko, Long-range nature of chemical interaction in solid-phase reactions: formation of martensite phases of an Au-Cd Alloy in Cd/Fe/Au film systems, Dokl. Phys. Chem. 431 (2010) 52–56, https://doi.org/10.1134/S0012501610030036.
[42] V.G. Myagkov, L.E. Bykova, G.N. Bondarenko, Multiple self-propagating high-temperature synthesis and solid-phase reactions in thin films, J. Exp. Theor. Phys. Lett. 88 (5) (1999) 963–967, https://doi.org/10.1134/1.558878.
[43] V.G. Myagkov, L.E. Bykova, G.N. Bondarenko, Superionic transition and self-propagating high-temperature synthesis of copper selenide in thin films, Dokl. Phys. 48 (5) (2003) 206–208, https://doi.org/10.1134/1.1581312.
[44] V.G. Myagkov, V.S. Zhigalov, A.A. Matsynin, L.E. Bykova, Yu L. Mikhlin, G.N. Bondarenko, G.S. Patrin, G. Yu Yurkin, Formation of ferromagnetic germanides by solid-state reactions in 20Ge/80Mn films, Thin Solid Films 552 (2014) 86–91, https://doi.org/10.1016/j.tsf.2013.12.029.
[45] V.G. Myagkov, L.E. Bykova, A.A. Matsynin, M.N. Volochaev, V.S. Zhigalov, I.A. Tambasov, Yu L. Mikhlin, D.A. Velikanov, G.N. Bondarenko, Solid state synthesis of $Mn_5Ge_3$ in Ge/Ag/Mn trilayers: structural and magnetic studies, J. Solid State Chem. 246 (2017) 379–387, https://doi.org/10.1016/j.jssc.2016.12.010.
[46] V.G. Myagkov, L.E. Bykova, G.N. Bondarenko, V.S. Zhigalov, Solid-phase synthesis of solid solutions in Cu/Ni(001) epitaxial nanofilms, JETP Lett. (Engl. Transl.) 88 (2008) 515–519, https://doi.org/10.1134/S0021364008200101.
[47] V.S. Zhigalov, V.G. Myagkov, O.A. Bayukov, L.E. Bykova, G.N. Bondarenko, A.A. Matsynin, Phase transformations in Mn/Fe(001) films: structural and magnetic investigations, JETP Lett. (Engl. Transl.) 89 (2009) 621–625, https://doi.org/10.1134/S0021364009120066.
[48] V.G. Myagkov, L.E. Bykova, V. Yu Yakovchuk, V.S. Zhigalov, M.N. Volochaev, A.A. Matsynin, I.A. Tambasov, V.A. Seredkin, G.S. Patrin, G.N. Bondarenko, Structural and magnetic features of solid-phase transformations in Mn/Bi and Bi/Mn films, JETP Lett. (Engl. Transl.) 103 (2016) 254–259, https://doi.org/10.1134/S0021364016040111.
[49] V. Myagkov, O. Bayukov, Y. Mikhlin, V. Zhigalov, L. Bykova, G. Bondarenko, Long-range chemical interactions in solid-state reactions: effect of an inert Ag interlayer on the formation of $L1_0$-FePd in epitaxial Pd(001)/Ag(001)/Fe(001) and Fe(001)/Ag(001)/Pd(001) trilayers, Phil. Mag. 94 (23) (2014) 2595–2622, https://doi.org/10.1080/14786435.2014.926037.
[50] V.G. Myagkov, L.E. Bykova, V.S. Zhigalov, I.A. Tambasov, G.N. Bondarenko, A.A. Matsynin, A.N. Rybakova, Solid_State synthesis, structural and magnetic properties of CoPd films, Phys. Solid State 57 (2015) 1014–1022, https://doi.org/10.1134/S1063783415050236.
[51] R.A. Ristau, K. Barmak, L.H. Lewis, K.R. Coffey, J.K. Howard, On the relationship of high coercivity and $L1_0$ ordered phase in CoPt and FePt thin films, J. Appl. Phys. 86 (1999) 4527–4533, https://doi.org/10.1063/1.371397.
[52] M. Ohtake, S. Ouchi, F. Kirino, M. Futamoto, $L1_0$ ordered phase formation in FePt, FePd, CoPt, and CoPd alloy thin films epitaxially grown on MgO(001) single-crystal substrates, J. Appl. Phys. 111 (2012), https://doi.org/10.1063/1.3672856, 07A708-1-07A708-3.
[53] H. Shima, K. Oikawa, A. Fujita, K. Fukamichi, K. nIshida, S. Nakamura, T. Nojima, Magnetocrystalline anisotropy energy in $L1_0$-type CoPt single crystals, J. Magn. Magn Mater. 290–291 (2005) 566–569, https://doi.org/10.1016/j.jmmm.2004.11.536.
[54] D. Alloyeau, C. Ricolleau, C. Mottet, T. Oikawa, C. Langlois, Y. Le Boua, N. Braidy, A. Loiseau, Size and shape effects on the order–disorder phase transition in CoPt nanoparticles, Nat. Mater. 8 (2009) 940–946, https://doi.org/10.1038/nmat2574.
[55] R.A. McCurrie, P. Gaunt, The magnetic properties of platinum cobalt near the equiatomic composition part I. the experimental data, Phil. Mag. 13 (1966) 567–577, https://doi.org/10.1080/14786436608212648.
[56] C. Leroux, M.C. Cadeville, V. Pierron-Bohnes, G. Inden, F. Hinz, Comparative investigation of structural and transport properties of $L1_0$ NiPt and CoPt phases; the role of magnetism, J. Phys. F Met. Phys. 18 (1988) 2033–2051, https://doi.org/10.1088/0305-4608/18/9/021.
[57] H. Okamoto, Supplemental literature review of binary phase diagrams: Au-La, Ce-Pt, Co-Pt, Cr-S, Cu-Sb, Fe-Ni, Lu-Pd, Ni-S, Pd-Ti, Si-Te, Ta-V, and V-Zn, J. Phase Equilibria Diffus. 40 (2019) 743–756, https://doi.org/10.1007/s11669-019-00760-w.
[58] V.G. Myagkov, A.A. Ivanenko, L.E. Bykova, V.S. Zhigalov, M.N. Volochaev, D.A. Velikanov, A.A. Matsynin, G.N. Bondarenko, Solid-state synthesis, magnetic and structural properties of interfacial B2-FeRh(001) layers in Rh/Fe(001) films, Sci. Rep. 10 (2020) 10807, https://doi.org/10.1038/s41598-020-67837-2.
[59] F. Liscio, M. Maret, C. Meneghini, S. Mobilio, O. Proux, D. Makarov, M. Albrecht, Structural origin of perpendicular magnetic anisotropy in epitaxial $CoPt_3$

nanostructures grown on $WSe_2$(0001), Phys. Rev. B 81 (2010), https://doi.org/10.1103/PhysRevB.81.125417, 125417-1 - 125417-9.
[60] C. Meneghini, M. Maret, V. Parasote, M.C. Cadeville, J.L. Hazemann, R. Cortes, S. Colonna, Structural origin of magnetic anisotropy in Co-Pt alloy films probed by polarized XAFS, Eur. Phys. J. B 7 (1999) 347–357, https://doi.org/10.1007/s100510050621.
[61] T.A. Tyson, S.D. Conradson, R.F.C. Farrow, B.A. Jones, Observation of internal interfaces in $Pt_xCo_{1-x}$ ($x \approx 0.7$) alloy films: a likely cause of perpendicular magnetic anisotropy, Phys. Rev. B 54 (1996) R3702–R3705, https://doi.org/10.1103/PhysRevB.54.R3702.
[62] M. Charilaou, C. Bordel, P.-E. Berche, B.B. Maranville, P. Fischer, F. Hellman, Magnetic properties of ultrathin discontinuous Co/Pt multilayers: comparison with short-range ordered and isotropic $CoPt_3$ films, Phys. Rev. B 93 (2016), https://doi.org/10.1103/Phys.RevB.93.224408, 224408-1 - 224408-10.
[63] P.W. Rooney, A.L. Shapiro, M.Q. Tran, F. Hellman, Evidence of a surface-mediated magnetically induced miscibility gap in Co-Pt alloy thin films, Phys. Rev. Lett. 75 (1995) 1843–1846, https://doi.org/10.1103/PhysRevLett.75.1843.
[64] K. Ullakko, J.K. Huang, C. Kantner, R.C. O'Handley, V.V. Kokorin, Large magnetic-field-induced strains in Ni2MnGa single crystals, Appl. Phys. Lett. 69 (1996) 1966–1968, https://doi.org/10.1063/1.117637.
[65] O. Heczko, A. Sozinov, K. Ullakko, Giant field-induced reversible strain in magnetic shape memory NiMnGa alloy, IEEE Trans. Magn. 36 (2000) 3266–3268, https://doi.org/10.1109/20.908764.
[66] A. Sozinov, N. Lanska, A. Soroka, W. Zou, 12% magnetic field-induced strain in Ni-Mn-Ga-based non-modulated martensite, Appl. Phys. Lett. 102 (2013), https://doi.org/10.1063/1.4775677. Article 021902-1 – 0219025.
[67] E. Pagounis, R. Chulist, J. Szczerba, M. Laufenberg, Over 7% magnetic field-induced strain in a Ni-Mn-Ga five-layered martensite, Appl. Phys. Lett. 105 (2014), https://doi.org/10.1063/1.4892633, 052405-1 - 052405-4.
[68] A. Sozinov, Likhachev, N. Lanska, K. Ullakko, Giant magnetic-field-induced strain in NiMnGa seven-layered martensitic phase, Appl. Phys. Lett. 80 (2002) 1746–1748, https://doi.org/10.1063/1.1458075.
[69] J. Pons, V.A. Chernenko, R. Santamarta, E. Cesari, Crystal structure of martensitic phases in Ni–Mn–Ga shape memory alloys, Acta Mater. 48 (2000) 3027–3038, https://doi.org/10.1016/S1359-6454(00)00130-0.
[70] Jiong Wang, Zhenyi Zhang, Variant reorientation in a single-crystalline Ni–Mn-Ga sample induced by a quasistatic rotating magnetic field: mechanism analyses based on configurational forces, J. Alloys Compd. 824 (2020), https://doi.org/10.1016/j.jallcom.2020.153940, 153940-153941-153940-17.
[71] A. Sozinov, Y. Ezer, G. Kimmel, P. Yakovenko, D. Giller, Y. Wolfus, Y. Yeshurun, K. Ullakko V.K. Lindroos, Large magnetic-field-induced strains in Ni-Mn-Ga alloys in rotating magnetic field, J. Phys. IV France 11 (2001), https://doi.org/10.1051/jp4:2001853. Pr8-311- Pr8-316.
[72] S.V. Kumar, S. Seenithural, M.M. Rala, M. Mahendran, Structural and magnetic properties of sputter-deposited polycrystalline Ni-Mn-Ga ferromagnetic shape-memory thin films, J. Electron. Mater. 44 (2015) 3761–3767, https://doi.org/10.1007/s11664-015-3819-0.
[73] S. Shevyrtalov, H. Miki, M. Ohtsuka, A. Grunin, I. Lyatun, A. Mashirov, M. Seredina, V. Khovaylo, V. Rodionova, Martensitic transformation in polycrystalline substrate-constrained and freestanding Ni-Mn-Ga films with Ni and Ga excess, J. Alloys Compd. 741 (2018) 1098–1104, https://doi.org/10.1016/j.jallcom.2018.01.255.
[74] Y. Li, E.K. Liu, G.H. Wu, W. Wang, Z. Liu, Structural, magnetic, and transport properties of sputtered hexagonal MnNiGa thin films, J. Appl. Phys. 116 (2014), https://doi.org/10.1063/1.4903943, 223906-1 - 223906-7.
[75] A. Hirohata, W. Frost, M. Samiepour, J.-y. Kim, Perpendicular magnetic anisotropy in heusler alloy films and their magnetoresistive junctions, Materials 11 (2018), https://doi.org/10.3390/ma11010105, 105-1 - 105-18.
[76] J. Dubowik, Y.V. Kudryavtsev, Y.P. Lee, Martensitic transformation in Ni2MnGa films: a ferromagnetic resonance study, J. Appl. Phys. 95 (2004) 2912–2917, https://doi.org/10.1063/1.1641956.
[77] A. Annadurai, A.K. Nandakumar, S. Jayakumar, M.D. Kannan, M.M. Raja, S. Bysak, R. Gopalan, V. Chandrasekaran, Composition, structure and magnetic properties of sputter deposited Ni–Mn–Ga ferromagnetic shape memory thin films, J. Magn. Magn Mater. 321 (2009) 630–634, https://doi.org/10.1016/j.jmmm.2008.10.015.
[78] A. Sharma, S. Mohan, S. Suwas, A/m the effect of the deposition rate on the crystallographic texture, microstructure evolution and magnetic properties in sputter deposited Ni-Mn-Ga thin films, Thin Solid Films 616 (2016) 530–542, https://doi.org/10.1016/j.tsf.2016.08.033.
[79] I.R. Aseguinolaza, I. Orue, A.V. Svalov, K. Wilson, P. Müllner, J.M. Barandiarán, V.A. Chernenko, Martensitic transformation in Ni–Mn–Ga/Si(100) thin films, Thin Solid Films 558 (2014) 449–454, https://doi.org/10.1016/j.tsf.2014.02.056.
[80] S.M. Ryabchenko, V.M. Kalita, M.M. Kulik, A.F. Lozenko, V.V. Nevdacha, A.N. Pogorily, A.F. Kravets, D.Y. Podyalovskiy, A. Ya Vovk, R.P. Borges, M. Godinho, V. Korenivski, Rotatable magnetic anisotropy in $Si/SiO_2/(Co_2Fe)_xGe_{1-x}$ Heusler alloy films, J. Phys. Condens. Matter 25 (2013), https://doi.org/10.1088/0953-8984/25/41/416003, 416003-1 - 416003-12.